

# Love-wave excitation due to the interaction between a propagating ocean wave and the sea-bottom topography

Tatsuhiko Saito

National Research Institute for Earth Science and Disaster Prevention, Tsukuba, Ibaraki, Japan. E-mail: [saito-ta@bosai.go.jp](mailto:saito-ta@bosai.go.jp)

Accepted 2010 June 8. Received 2010 June 7; in original form 2010 January 6

## SUMMARY

This study formulates Love-wave excitation in terms of the interaction between a propagating ocean wave and the sea-bottom topography. By assuming a Fraunhofer diffraction range, or far-field approximation, I theoretically derive an equivalent point force for the Love-wave excitation. The equivalent point force acts in the same direction as the propagation direction of the ocean wave. The excited Love wave has a radiation pattern characterized by  $\sin \theta$ , where  $\theta$  is the angle between the propagation directions of the Love and ocean waves. The efficiency of the excitation is then investigated by employing both deterministic and stochastic models for sea-bottom topography. When a seamount given by a Gaussian function is used as a deterministic model, the equivalent point force has a narrow peak against the wavenumber of the ocean wave; a strong interaction occurs at  $\lambda = 2.2d$ , where  $\lambda$  is the ocean-wave wavelength and  $d$  is the characteristic scale of the seamount. On the other hand, when randomly fluctuating sea-bottom topography characterized by a power-law spectrum is used, the interaction can occur over a wide range of the ocean wave wavelength.

**Key words:** Surface waves and free oscillations; Theoretical seismology; Wave propagation.

## 1 INTRODUCTION

Earthquakes excite oscillations of the Earth. High-sensitivity sensors have revealed that the oscillation, or seismic wave, can have causes other than earthquakes. Ocean waves generate microseisms, or small and continuous seismic signals with the period of 3–20 s. By analysing the microseisms recorded by a Gräfenberg array (GFR array, Harjes & Seidl 1978) in Germany, Friederich *et al.* (1998) showed the wave was composed of both Rayleigh and Love waves generated from various regions in the Atlantic Ocean, the Arctic Sea and the Mediterranean Sea. They discussed the excitation mechanism relating to the ocean swell and its interaction with sea-bottom topography. In 2007 March, tiltmeters of Hi-net, a nationwide seismic network in Japan (Obara 2002) detected anomalous signals with a dominant period of approximately 20 s. By analysing the signals together with records of a GFR array, Matsuzawa *et al.* (2008) determined that the signals were composed of both Rayleigh and Love waves radiating from a source located in the Atlantic Ocean. They identified the migration path of the source, which roughly corresponded to the path of a cyclone during this period. This suggests that the ocean swell induced by the cyclone generated Rayleigh and Love waves. Also, when hurricane Katrina struck land during 2005 August around the Gulf of Mexico, broad-band seismic stations in Southern California detected seismic signals from the hurricane. Gerstoft *et al.* (2006) carefully analysed records over various frequency bands and found body and surface waves in these records.

Another example is found in the Earth's background free oscillation. Rayleigh waves from 2 to 20 mHz (Kobayashi & Nishida 1998; Nawa *et al.* 1998; Suda *et al.* 1998; Tanimoto *et al.* 1998; Nishida & Kobayashi 1999) and Love waves below 0.01 Hz (Kurrle & Widmer-Shnidrig 2008) and from 0.01 to 0.1 Hz (Nishida *et al.* 2008) are continuously observed, irrespective of the occurrence of earthquakes. These waves are referred to as the background-free oscillation or the Earth's hum. The estimated distribution of the excitation sources indicates that the sources are weaker in continental regions than in ocean regions, and they exhibit clear seasonal variation (Rhie & Romanovicz 2004; Nishida & Fukao 2007). Although the search for the excitation mechanism of the background oscillation has been inconclusive (Fukao *et al.* 2002; Tanimoto 2005; Webb 2008), ocean loading is considered to be a strong candidate (e.g. Rhie & Romanovicz 2004, 2006; Kurrle & Widmer-Shnidrig 2008; Nishida *et al.* 2008).

The pressure from ocean waves loads on the sea bottom, which excites the seismic oscillation (Longuet-Higgins 1950; Hasselman 1963; Tanimoto 2005, 2007; Webb 2008). When a flat sea bottom is assumed, the normal traction acting on the sea bottom excites Rayleigh waves, but the lack of shear traction fails to excite Love waves. To simulate Love-wave excitation, Fukao *et al.* (2010) have recently proposed a reasonable model whereby, when there exists sea-bottom fluctuations, ocean waves can generate shear traction on the sea bottom and excite

Love waves. They assumed no preferred directivity in the total excited Love wave supposing randomly and homogeneously distributed sources.

Although the assumption of randomly and homogeneously distributed sources is a good approximation in the first instance, it may not always be valid if we take into account a realistic distribution of the excitation sources (Rhie & Ramonowicz 2004; Nishida & Fukao 2007). Furthermore, for the case of a cyclone-induced microseism (Friederich *et al.* 1998; Gerstoft *et al.* 2006; Matsuzawa *et al.* 2008), we should model the source as a point source rather than considering randomly homogeneously distributed sources. To apply the theory to the above cases, or to deeply understand the Love-wave excitation due to ocean waves, we need to develop a sound mathematical basis for the shear traction excitation mechanism by rigorously taking the directions of wave propagation and the gradient of the sea-bottom topography into account, whereas those directions for 2-D sea-bottom topography have not been rigorously included in the past.

This study formulates the Love-wave excitation in terms of the interaction between a propagating ocean wave and the sea-bottom topography. Assuming a Fraunhofer diffraction range, or far-field approximation, I theoretically derive an equivalent point force for the excited Love wave, and show that the equivalent point force acts in the same direction as the propagation direction of the ocean wave. Additionally, we derive some important properties of the excited Love wave using both deterministic and stochastic models for the sea-bottom topography.

## 2 LOVE-WAVE EXCITATION DUE TO THE INTERACTION BETWEEN THE SEA-BOTTOM TOPOGRAPHY AND A PROPAGATING OCEAN WAVE

We use Cartesian coordinates (Fig. 1a) taking the  $z$ -axis in the vertically downward direction and the  $x$ - and  $y$ -axes in a horizontal plane. The average or background water depth is  $h_0$ . As shown in Fig. 1(b), the sea-bottom fluctuation is assumed to exist only within the extent of  $L$  around  $(0, 0, h_0)$ . A plane ocean wave propagating along the  $x$ -axis interacts with the sea-bottom fluctuation and excites a Love wave.

### 2.1 Ocean wave propagation

Assuming incompressible and irrotational water flow, we use linear potential theory to describe the motion in the ocean (e.g. Stoker 1958; Saito & Furumura 2009b). The velocity potential  $\phi$  satisfies the Laplace equation,

$$\Delta\phi = 0, \tag{1}$$

the boundary conditions at the surface are given by

$$\frac{\partial\phi}{\partial t} - g_0\eta = 0 \quad \text{for } z = 0, \tag{2}$$

$$\frac{\partial\phi}{\partial z} = \frac{\partial\eta}{\partial t} \quad \text{for } z = 0, \tag{3}$$

and the boundary condition at the bottom for constant water depth by

$$\frac{\partial\phi}{\partial z} = 0 \quad \text{for } z = h_0, \tag{4}$$

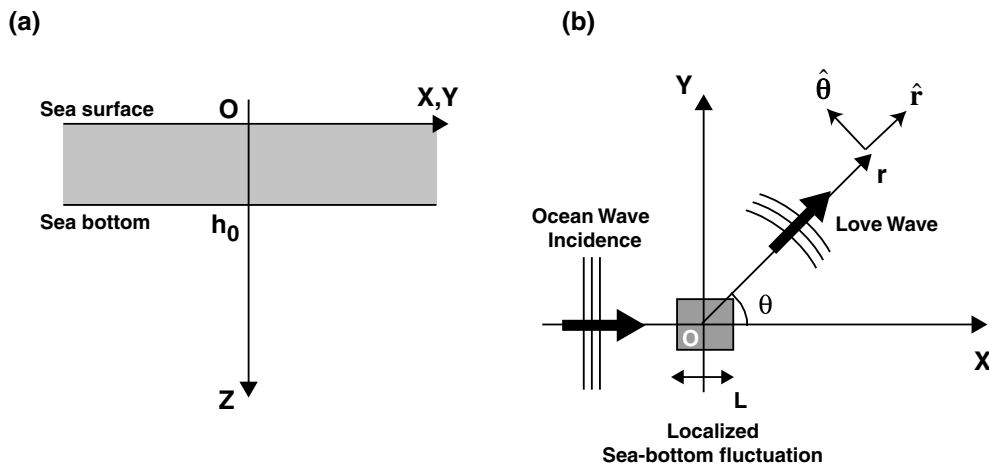


**Figure 1.** Coordinates for Love wave excitation due to the interaction between ocean wave and sea-bottom topography. (a) The  $x$  and  $y$ -axes are in a horizontal plane and the  $z$ -axis is pointing vertically downwards. (b) A plane ocean wave propagating along the  $x$ -axis interacts with the localized sea-bottom topography with extent  $L$ .

where  $g_0$  is gravitational acceleration and  $\eta(x, y, t)$  is the vertical displacement at the sea surface, or ocean wave. When an ocean wave  $\eta(x, y, t)$  is propagating along the  $x$ -axis as a plane wave,

$$\eta(x, y, t) = \eta_0 \exp[-i(\omega t - kx)], \quad (5)$$

the velocity potential  $\phi$  is given by

$$\phi(x, y, z, t) = \frac{g_0 \eta_0 \cosh[k(h_0 - z)]}{-i\omega \cosh kh_0} \exp[-i(\omega t - kx)], \quad (6)$$

where  $k$  is the wavenumber of the ocean wave. The dispersion relation is given by  $\omega^2 = g_0 k \tanh kh_0$ . The ocean wave causes excess pressure at the sea bottom.

$$p_e(x, y, h_0) = -\rho_0 \frac{\partial \phi(x, y, h_0)}{\partial t} = \frac{-\rho_0 g_0 \eta_0}{\cosh kh_0} \exp[-i(\omega t - kx)], \quad (7)$$

where  $\rho_0$  is the water density. We then allow the water depth  $h$  to depend on the location. The water depth is given by  $h(x, y) = h_0 + h_1 \xi(x, y)$ . The fluctuation  $\xi$  is localized around  $r = \sqrt{x^2 + y^2} \sim 0$  within the size of  $L$ ; the fluctuation vanishes ( $\xi = 0$ ) outside the region (Fig. 1b). The unit normal vector with respect to the sea bottom  $z = h(x, y)$  is given by,  $\hat{\mathbf{n}}(x, y) = C_0(\partial h/\partial x \hat{\mathbf{x}} + \partial h/\partial y \hat{\mathbf{y}} - \hat{\mathbf{z}})$ , where  $C_0 = [1 + (\partial h/\partial x)^2 + (\partial h/\partial y)^2]^{-1/2}$ ,  $\hat{\mathbf{x}}$ ,  $\hat{\mathbf{y}}$  and  $\hat{\mathbf{z}}$  are unit basis vectors for the  $x$ ,  $y$  and  $z$  coordinates, respectively. The traction excited by the excess pressure on  $z = h(x, y)$  then given by  $-p_e \hat{\mathbf{n}}$ . When the gradient of the sea-bottom fluctuation is small ( $|\hat{\mathbf{n}} \cdot \nabla \xi| \ll 1$ ), the horizontal traction on the horizontal plane of  $z = h_0$  is approximately given by

$$\begin{aligned} \mathbf{T}(x, y, h_0) &\approx -p_e(x, y, h_0) h_1 \nabla \xi(x, y) \\ &= \frac{\rho_0 g_0 \eta_0 h_1}{\cosh kh_0} \exp[-i(\omega t - kx)] \nabla \xi, \end{aligned} \quad (8)$$

where  $\nabla = \partial/\partial x \hat{\mathbf{x}} + \partial/\partial y \hat{\mathbf{y}}$  is the gradient in the horizontal  $(x, y)$  plane. Eq. (8) represents the horizontal traction produced by the interaction between the ocean wave and the sea-bottom fluctuation, which acts as a moving source for Love wave excitation.

## 2.2 Love-wave excitation and propagation

We consider a Love wave using cylindrical coordinates  $(r, \theta, z)$  (Fig. 1b). When a point force  $\mathbf{F} \exp[-i\omega t]$  is applied at  $r = 0$  and  $z = h_0$ , the resulting Love wave is approximately given by

$$\mathbf{u}^{\text{LOVE}}(r, \theta, z, t) \approx \exp[-i\omega t] \sum_n \frac{l_1(k_n, h_0, \omega) [l_1(k_n, z, \omega) \hat{\boldsymbol{\theta}}]}{8cU I_1} \sqrt{\frac{2}{\pi k_n r}} (\mathbf{F} \cdot \hat{\boldsymbol{\theta}}) \exp\left[i\left(k_n r + \frac{\pi}{4}\right)\right], \quad (9)$$

(e.g. Snieder 1986; Aki & Richards 2002). In eq. (9),  $\hat{\boldsymbol{\theta}} (= -\sin\theta \hat{\mathbf{x}} + \cos\theta \hat{\mathbf{y}})$  is the unit basis vector for the  $\theta$  coordinate. The parameter  $k_n$  is the wavenumber,  $c$  is the phase velocity,  $U$  is the group velocity,  $l_1(k_n, z, \omega)$  is an eigenfunction of the Love wave and  $I_1 = 1/2 \int_{-\infty}^{\infty} \rho [l_1(k_n, z, \omega)]^2 dz$ . When the horizontal traction  $\mathbf{T}(x, y, t) = \mathbf{T}'(x, y) \exp[-i\omega t]$  is distributed within the size of  $L$  around  $r = 0$  (Fig. 1b), Love waves at  $r \gg L$  are approximately given by

$$\begin{aligned} \mathbf{u}^{\text{LOVE}}(r, \theta, z, t) &\approx \exp[-i\omega t] \sum_n \frac{l_1(k_n, h_0, \omega) [l_1(k_n, z, \omega) \hat{\boldsymbol{\theta}}]}{8cU I_1} \\ &\times \iint_{-\infty}^{\infty} \iint_{-\infty}^{\infty} \sqrt{\frac{2}{\pi k_n |\mathbf{r} - \mathbf{r}'|}} (\mathbf{T}'(x', y') \cdot \hat{\boldsymbol{\theta}}) \exp\left[i\left(k_n |\mathbf{r} - \mathbf{r}'| + \frac{\pi}{4}\right)\right] dx' dy', \end{aligned} \quad (10)$$

where  $\mathbf{r} = x\hat{\mathbf{x}} + y\hat{\mathbf{y}}$  and  $\mathbf{r}' = x'\hat{\mathbf{x}} + y'\hat{\mathbf{y}}$ . When the observed distance  $r$  is far away from the source region  $L$  ( $r \gg L$ ), we may make the approximation  $|\mathbf{r} - \mathbf{r}'| \approx r$  in the denominator in eq. (10). We take diffraction into account by approximating  $|\mathbf{r} - \mathbf{r}'| \approx r - \hat{\mathbf{f}} \cdot \mathbf{r}'$  in the exponent where  $\hat{\mathbf{f}}$  is the unit basis vector for the  $r$ -axis. This approximation is valid when  $r \gg \pi^{-1} L^2 k_n$ , which corresponds to the region of Fraunhofer diffraction in optics (e.g. p. 45, Chernov 1960). Then, substituting eq. (8) into eq. (10), we calculate thus

$$\begin{aligned} \mathbf{u}^{\text{LOVE}}(r, \theta, z, t) &\approx \exp[-i\omega t] \sum_n \frac{l_1(k_n, h_0, \omega) [l_1(k_n, z, \omega) \hat{\boldsymbol{\theta}}]}{8cU I_1} \frac{\rho_0 g_0 \eta_0 h_1}{\cosh kh_0} \\ &\times \iint_{x', y'} \sqrt{\frac{2}{\pi k_n |\mathbf{r} - \mathbf{r}'|}} \exp\left[i\left(k_n |\mathbf{r} - \mathbf{r}'| + \frac{\pi}{4}\right)\right] \left(-\frac{\partial \xi(x', y')}{\partial x'} \sin\theta + \frac{\partial \xi(x', y')}{\partial y'} \cos\theta\right) \exp[ikx'] dx' dy' \\ &\approx \exp[-i\omega t] \sum_n \frac{l_1(k_n, h_0, \omega) [l_1(k_n, z, \omega) \hat{\boldsymbol{\theta}}]}{8cU I_1} \sqrt{\frac{2}{\pi k_n r}} \exp\left[i\left(k_n r + \frac{\pi}{4}\right)\right] \frac{\rho_0 g_0 \eta_0 h_1}{\cosh kh_0} \\ &\times \iint_{x', y'} \left(-\frac{\partial \xi(x', y')}{\partial x'} \sin\theta + \frac{\partial \xi(x', y')}{\partial y'} \cos\theta\right) \exp[i\{k\hat{\mathbf{x}} \cdot \mathbf{r}' - k_n \hat{\mathbf{f}} \cdot \mathbf{r}'\}] dx' dy'. \end{aligned} \quad (11)$$

Introducing the difference wavenumber between the Love and oceanic waves as  $\mathbf{K} = k_n \hat{\mathbf{r}} - k \hat{\mathbf{x}}$  and performing integration by parts with respect to  $x'$  and  $y'$ , we finally obtain

$$\begin{aligned} \mathbf{u}^{\text{LOVE}}(r, \theta, z, t) &\approx \exp[-i\omega t] \sum_n \frac{l_1(k_n, h_0, \omega) [l_1(k_n, z, \omega) \hat{\boldsymbol{\theta}}]}{8cUI_1} \sqrt{\frac{2}{\pi k_n r}} \exp\left[i\left(k_n r + \frac{\pi}{4}\right)\right] \frac{\rho_0 g_0 \eta_0 h_1}{\cosh kh_0} \\ &\quad \times i(-K_x \sin \theta + K_y \cos \theta) \int_{-\infty}^{\infty} \int_{-\infty}^{\infty} \xi(x', y') \exp[-i\mathbf{K} \cdot \mathbf{r}'] \, d\mathbf{r}' \\ &= \exp[-i\omega t] \sum_n \frac{l_1(k_n, h_0, \omega) [l_1(k_n, z, \omega) \hat{\boldsymbol{\theta}}]}{8cUI_1} \sqrt{\frac{2}{\pi k_n r}} \exp\left[i\left(k_n r + \frac{\pi}{4}\right)\right] \\ &\quad \times \frac{i\rho_0 g_0 \eta_0 h_1}{\cosh kh_0} (\mathbf{K} \cdot \hat{\boldsymbol{\theta}}) \hat{\xi}(\mathbf{K}), \end{aligned} \tag{12}$$

where  $\hat{\xi}(\mathbf{K})$  is the 2-D spatial Fourier transform in  $(x, y)$  coordinates of the sea-bottom fluctuation,

$$\hat{\xi}(\mathbf{K}) = \int_{-\infty}^{\infty} \int_{-\infty}^{\infty} \xi(\mathbf{r}') \exp[-i\mathbf{K} \cdot \mathbf{r}'] \, d\mathbf{r}'. \tag{13}$$

Eq. (12) is the equation for a Love wave generated by the interaction between an ocean wave and the sea-bottom topography.

### 3 LOVE WAVE

#### 3.1 Equivalent point force

For the Love-wave excitation due to the interaction between an ocean wave and fluctuating sea-bottom topography, we obtain an equivalent horizontal force applied at  $r = 0$  and  $z = h_0$ .

$$\mathbf{F}_{\text{equivalent}} = \frac{i\rho_0 g_0 \eta_0 h_1}{\cosh kh_0} \hat{\xi}(\mathbf{K}) \mathbf{K}, \tag{14}$$

by comparing eq. (12) and eq. (9). Considering that the ocean wave propagates much more slowly than the Love wave, we may make the approximation  $\mathbf{K} = k_n \hat{\mathbf{r}} - \mathbf{k} \approx -\mathbf{k} = -k \hat{\mathbf{x}}$  and obtain

$$\mathbf{F}_{\text{equivalent}} \approx \frac{-i\rho_0 g_0 \eta_0 k h_1}{\cosh kh_0} \hat{\xi}(-k \hat{\mathbf{x}}) \hat{\mathbf{x}}. \tag{15}$$

Eq. (15) indicates that the equivalent body force acts in the same direction as the propagation direction of the ocean wave (Fig. 2).

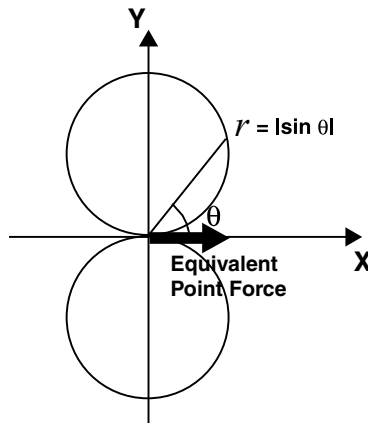


**Figure 2.** Equivalent point force for the Love wave excitation. The equivalent point force is striking in the same direction as the propagation direction of the ocean wave. The radiation pattern of the Love wave is given by  $\sin \theta$  where  $\theta$  is the angle between the propagation directions of the Love wave and the ocean wave.

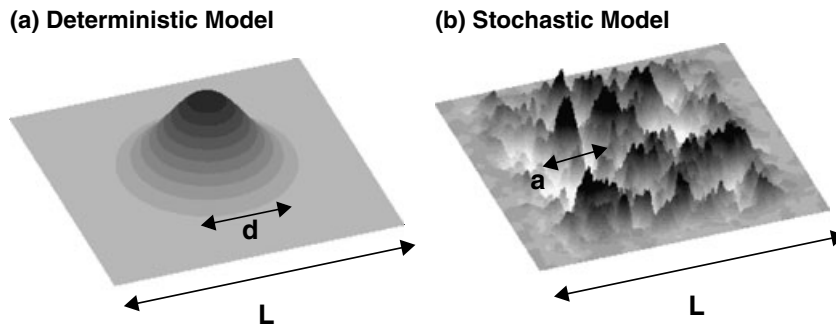


**Figure 3.** Two models for sea-bottom topography. (a) A seamount is modelled by the Gaussian function. It is referred to as the deterministic model. (b) The randomly fluctuating sea bottom is modelled by a stochastic parameter  $\xi$ . The statistical features of  $\xi$  can be defined by introducing its ensemble  $\{\xi(\mathbf{x})\}$ . It is referred to as a stochastic model.

### 3.2 Radiation pattern and the amplitude of the Love wave

From eq. (12), we obtain

$$\begin{aligned} \mathbf{u}^{\text{LOVE}}(r, \theta, z, t) &= \exp[-i\omega t] \sum_n \frac{l_1(k_n, h_0, \omega) [l_1(k_n, z, \omega) \hat{\boldsymbol{\theta}}]}{8cU I_1} \sqrt{\frac{2}{\pi k_n r}} \exp\left[i\left(k_n r + \frac{\pi}{4}\right)\right] \\ &\quad \times \frac{i\rho_0 g_0 \eta_0 k h_1}{\cosh k h_0} \hat{\xi}(k_n \hat{\mathbf{r}} - k \hat{\mathbf{x}}) \sin \theta \\ &\approx \exp[-i\omega t] \sum_n \frac{l_1(k_n, h_0, \omega) [l_1(k_n, z, \omega) \hat{\boldsymbol{\theta}}]}{8cU I_1} \sqrt{\frac{2}{\pi k_n r}} \exp\left[i\left(k_n r + \frac{\pi}{4}\right)\right] \\ &\quad \times \frac{i\rho_0 g_0 \eta_0 k h_1}{\cosh k h_0} \hat{\xi}(-k \hat{\mathbf{x}}) \sin \theta \quad \text{for } k \gg k_n. \end{aligned} \quad (16)$$

The radiation pattern or the dependence on the angle  $\theta$  appears as  $\sin \theta \hat{\xi}(k_n \hat{\mathbf{r}} - k \hat{\mathbf{x}})$  in the second equation in eq. (16). Considering that the ocean wave is much slower than the Love wave ( $k \gg k_n$ ), the radiation pattern of the Love wave can be simplified to  $\sin \theta$  in the last equation of eq. (16). The Love wave propagating perpendicular to the propagation direction of the ocean wave shows the largest amplitude, while no Love wave radiates towards the propagation direction of the ocean wave (Fig. 2).

Whereas the radiation pattern is independent of the wavenumber of the ocean wave, the amplitude depends on the wavenumber. The factor  $1/\cosh k h_0 = 1/\cosh[2\pi h_0/\lambda]$  where  $\lambda = 2\pi/k$  in eq. (16) indicates the relation between the water depth  $h_0$  and the ocean wave wavelength  $\lambda$ . The value of  $1/\cosh[2\pi h_0/\lambda]$  increases with increasing wavelength and takes its maximum value of 1 when the wavelength is much greater than the water depth. Fukao *et al.* (2010) refer to it as the hydrodynamic filtering effect. The factor  $k h_1 \hat{\xi}(-k \hat{\mathbf{x}})$  in the last equation of eq. (16) indicates the relation between the ocean wave wavelength and the size of the sea-bottom fluctuation. Fukao *et al.* (2010) referred to this effect as the topographic coupling effect and investigated it for a circular cone hill. This study also investigates effects but utilizes two modelling approaches for the sea-bottom fluctuation. The first approach is deterministic. We suppose a seamount represented by a Gaussian function (Fig. 3a). The second approach is stochastic, where we suppose a randomly fluctuating sea-bottom topography (Fig. 3b).

#### 3.2.1 Deterministic model: a seamount

We use the Gaussian function

$$\xi(x, y) = \exp\left[-\frac{x^2 + y^2}{(d/2)^2}\right] \quad (17)$$

for modelling a seamount. This is very similar to the circular cone hill investigated by Fukao *et al.* (2010) in the sense that it has a single characteristic scale of  $d$  as diameter. The difference is that an analytical solution is obtained without approximations when the Gaussian function is used. The 2-D Fourier transform [eq. (13)] of eq. (17) is given by

$$\hat{\xi}(\mathbf{m}) = \frac{\pi d^2}{4} \exp\left[-\frac{d^2 m^2}{16}\right], \quad (18)$$

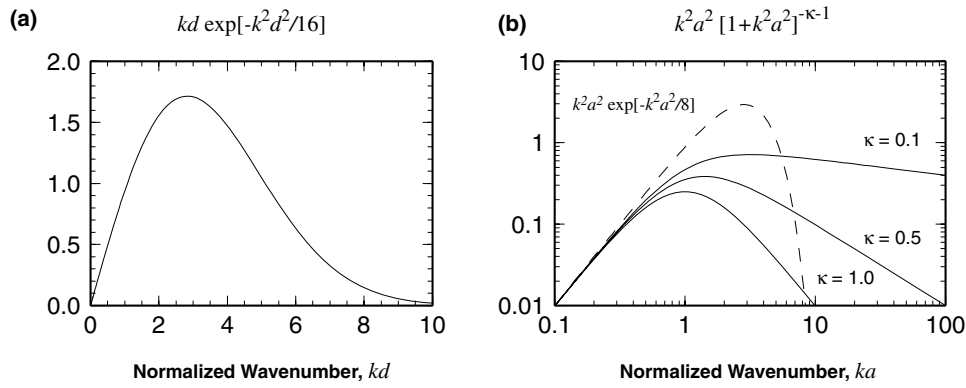


**Figure 4.** Functions (a)  $kd \exp[-k^2 d^2 / 16]$  and (b)  $k^2 a^2 (1 + k^2 a^2)^{-\kappa - 1}$ . The function  $\{ka \exp[-k^2 a^2 / 16]\}^2$  is also plotted with a dashed line for comparison in (b).

where  $m = |\mathbf{m}|$  is the wavenumber of the sea-bottom fluctuation. Substituting eq. (18) into eq. (16), we obtain

$$\begin{aligned}
 \mathbf{u}^{\text{LOVE}}(r, \theta, z, t) &\approx \exp[-i\omega t] \sum_n \frac{l_1(k_n, h_0, \omega) [l_1(k_n, z, \omega) \hat{\boldsymbol{\theta}}]}{8cU I_1} \sqrt{\frac{2}{\pi k_n r}} \exp\left[i\left(k_n r + \frac{\pi}{4}\right)\right] \\
 &\times \frac{e^{-i\pi/2} \rho_0 g_0 \eta_0 \pi d^2}{4} \frac{kh_1}{\cosh kh_0} \exp\left[-\frac{k^2 d^2}{16}\right] \sin \theta \\
 &= \exp[-i\omega t] \sum_n \frac{l_1(k_n, h_0, \omega) [l_1(k_n, z, \omega) \hat{\boldsymbol{\theta}}]}{8cU I_1} \sqrt{\frac{2}{\pi k_n r}} \exp\left[i\left(k_n r + \frac{\pi}{4}\right)\right] \\
 &\times \frac{e^{-i\pi/2} \varepsilon_1 \rho_0 g_0 \eta_0 \pi d^2}{4} \frac{kd}{\cosh kh_0} \exp\left[-\frac{k^2 d^2}{16}\right] \sin \theta, \tag{19}
 \end{aligned}$$

where we assume a scaling  $h_1 = \varepsilon_1 d$  of the seamount. The factor  $kd \exp[-k^2 d^2 / 16]$  represents the interaction between the ocean wave and the seamount. Fig. 4(a) shows the function of  $kd \exp[-k^2 d^2 / 16]$  against the wavenumber of the ocean wave normalized by the diameter,  $kd$ . The function takes its maximum value when  $kd = 2\sqrt{2} \approx 2.8$ . In other words, the strong interaction between the ocean wave and the seamount generates the largest equivalent point force when the ocean wave has a wavelength approximately twice the diameter of the seamount:  $\lambda \sim 2.2d$ .

### 3.2.2 Stochastic model: randomly fluctuating sea-bottom topography

Stochastic approaches can be a very powerful tool in investigating complicated features in the observations. For investigating the bathymetry (e.g. Fox & Hayes 1985) and its interaction with waves (e.g. Carrier 1970; Mysak 1978), stochastic approaches have often been employed. We employ a stochastic method and assume here that the sea bottom is fluctuating randomly in space (Fig. 3b). To simulate the fluctuation stochastically, an ensemble of the fluctuation  $\{\xi(\mathbf{x})\}$  is introduced. We also assume that the ensemble average of the fluctuation is zero  $\langle \xi(\mathbf{x}) \rangle = 0$ , where the ensemble average is denoted by  $\langle \cdot \rangle$ . The statistical properties of the fluctuation are characterized by the autocorrelation function (ACF),  $R(\mathbf{x}_d) = \langle \xi(\mathbf{x}) \xi(\mathbf{x} + \mathbf{x}_d) \rangle$ , or the power spectral density function (PSDF),  $P(\mathbf{m}) = \iint R(\mathbf{x}_d) \exp[-i\mathbf{m} \cdot \mathbf{x}_d] d\mathbf{x}_d$  (e.g. Sato & Fehler 1998).

A statistical property of the Love wave can be represented by the mean-square ensemble average,

$$\begin{aligned}
 \langle |\mathbf{u}^{\text{LOVE}}|^2 \rangle &\approx \sin^2 \theta \sum_n \frac{l_1(k_n, h_0, \omega)^2 l_1(k_n, z, \omega)^2}{64c^2 U^2 I_1^2} \frac{2}{\pi k_n r} \frac{\rho_0^2 g_0^2 \eta_0^2 (kh_1)^2}{\cosh^2 kh_0} \left\langle \left| \hat{\xi}(-k\hat{\mathbf{x}}_1) \right|^2 \right\rangle \\
 &= \sin^2 \theta \sum_n \frac{l_1(k_n, h_0, \omega)^2 l_1(k_n, z, \omega)^2}{64c^2 U^2 I_1^2} \frac{2}{\pi k_n r} \frac{\rho_0^2 g_0^2 \eta_0^2 (kh_1)^2}{\cosh^2 kh_0} L^2 P(-k\hat{\mathbf{x}}_1), \tag{20}
 \end{aligned}$$

where the relation  $L^2 P(\mathbf{m}) = \langle |\hat{\xi}(\mathbf{m})|^2 \rangle$  is used. Eq. (20) represents the relation between the PSDF of the sea-bottom fluctuation and the mean-square amplitude of the Love wave.

The PSDF of the sea-bottom fluctuation is well characterized by a power law (e.g. Fox & Hayes 1985; Goff & Jordan 1988; Turcotte 1989). As example, we consider the isotropic PSDF  $P(\mathbf{m}) = P(m)$  characterized by the von Karman type PSDF which also indicating a power law at large wavenumbers (e.g. Goff & Jordan 1988; Sato & Fehler 1998),

$$P(m) = \frac{4\pi \varepsilon^2 a^2}{(1 + a^2 m^2)^{\kappa+1}} \approx 4\pi \kappa \varepsilon^2 a^{-2\kappa} m^{-2\kappa-2} \quad \text{for } am \gg 1 \tag{21}$$

where  $\varepsilon$  represents the rms value of the fluctuation  $\xi$ , and  $a$  is the correlation distance ( $a < L$ ). The order  $\kappa$  controls the power of the PSDF at larger wavenumbers ( $am \gg 1$ ). A small  $\kappa$  increases the PSDF at larger wavenumbers, which makes the fluctuation of the sea bottom

rougher. The studies using the von Karman-type PSDF reported that the value of  $\kappa$  ranges between 0.5 and 1.0 for the sea-bottom fluctuation (Goff & Jordan 1988, Goff & Tucholke 1997). Substituting eq. (21) into eq. (20) we obtain

$$\begin{aligned} \langle |\mathbf{u}^{\text{LOVE}}|^2 \rangle &\approx \sin^2 \theta \sum_n \frac{I_1(k_n, h_0, \omega)^2 I_1(k_n, z, \omega)^2}{64c^2 U^2 I_1^2} \frac{2}{\pi k_n r} \frac{\rho_0^2 g_0^2 \eta_0^2 (kh_1)^2}{\cosh^2 kh_0} L^2 \frac{4\pi \varepsilon^2 a^2}{(1+k^2 a^2)^{\kappa+1}} \\ &= \sin^2 \theta \sum_n \frac{I_1(k_n, h_0, \omega)^2 I_1(k_n, z, \omega)^2}{64c^2 U^2 I_1^2} \frac{2}{\pi k_n r} \rho_0^2 g_0^2 \eta_0^2 L^2 a^2 \frac{1}{\cosh^2 kh_0} \frac{4\pi \varepsilon^2 \varepsilon_1^2 k^2 a^2}{(1+k^2 a^2)^{\kappa+1}}, \quad (22) \\ &\propto \begin{cases} 4\pi \varepsilon^2 \varepsilon_1^2 k^2 a^2 & \text{for } ka \ll 1 \\ 4\pi \varepsilon^2 \varepsilon_1^2 (ka)^{-2\kappa} & \text{for } ka \gg 1 \end{cases}, \end{aligned}$$

where we use the scaling  $h_1 = \varepsilon_1 a$  for the sea-bottom fluctuation. The factor  $4\pi \varepsilon^2 \varepsilon_1^2 k^2 a^2 (1+k^2 a^2)^{-\kappa-1}$  represents the interaction between the ocean wave and the sea-bottom fluctuation. Fig. 4(b) depicts the factor  $k^2 a^2 (1+k^2 a^2)^{-\kappa-1}$  against the wavenumber of the ocean wave normalized by the correlation distance,  $ka$ . The factor is proportional to  $k^2 a^2$  irrespective of the value of  $\kappa$  when the normalized wavenumber is small ( $ka \ll 1$ ). On the other hand, when the normalized wavenumber is large, the factor depends on  $\kappa$  such that  $4\pi \varepsilon^2 \varepsilon_1^2 k^2 a^2 (1+k^2 a^2)^{-\kappa-1} \approx 4\pi \varepsilon^2 \varepsilon_1^2 (ka)^{-2\kappa}$ . When  $\kappa$  is 1.0, the excitation has a peak against the normalized wavenumber as in the case of a seamount. Note that the function obeying a power law in large wavenumbers (solid lines in Fig. 4b) shows gradual decrease against the wavenumber compared to the case of the Gaussian PSDF (dashed line in Fig. 4b). Hence, the interaction occurs over a wider range of the wavenumber for the case of randomly fluctuating sea-bottom topography characterized by the von Karman-type PSDF than the seamount given by the Gaussian function. When  $\kappa$  becomes small, dependence on the wavenumber becomes weaker and the interaction occurs over a wider range of the wavenumber. The value of  $\kappa$  usually ranges between 0.5 and 1.0 for the sea-bottom fluctuation (Goff & Jordan 1988, Goff & Tucholke 1997). As an extreme case of  $\kappa = 0$ , the value of  $4\pi \varepsilon^2 \varepsilon_1^2 k^2 a^2 (1+k^2 a^2)^{-\kappa-1}$  becomes constant for the larger wavenumbers ( $ka \gg 1$ ).

#### 4 DISCUSSION

This study consistently took the force direction into account for 2-D bathymetry  $\xi(x, y)$ , and successfully derived the analytical representation of the equivalent shear traction for any sea-bottom fluctuation distribution  $\xi(x, y)$  [eq. (15)]. The equivalent point force is, in general, a complex number allowing phase shift and acting in the same direction as the propagation direction of the ocean wave. Those are theoretically derived for the first time in this study. The direction of the equivalent point force then leads that the radiation pattern of the Love wave is always  $\sin \theta$ . It may be surprising that the radiation pattern is independent of the sea-bottom topography  $\xi(x, y)$  [see eq. (16)]. This simple pattern comes from the fact that the ocean wave is propagated much more slowly than the Love wave ( $k \gg k_n$ ). If we cannot approximate  $\mathbf{K}$  by  $\mathbf{k}$  in  $\hat{\xi}(\mathbf{K})$  in eq. (16), the radiation pattern then depends on the sea-bottom fluctuation  $\xi(x, y)$  and also on the wavenumber of the Love wave. A situation where we cannot approximate  $\mathbf{K}$  by  $\mathbf{k}$  occurs with wave scattering (e.g. Snieder 1986; Maeda *et al.* 2008); the incident and radiated waves propagate with the same (or nearly the same) velocity. Saito & Furumura (2009a) theoretically investigate tsunami (long-wavelength ocean wave) scattering.

It should be noted that the formulation of this study has employed some assumptions. The gradient of the bathymetry is small,  $|h_1 \nabla \xi| \ll 1$  in eq. (8), the far field approximation  $r \gg L$  and flat free surface are assumed for the Green's function of the Love wave (eq. 9), the sea-bottom fluctuation is localized within the size of  $L$  and the Fraunhofer diffraction range  $r \gg \pi^{-1} L^2 k_n$  is supposed in the calculation. Among those approximations, the far field approximations including the Fraunhofer diffraction range would be acceptable in many occasions because we divide the source region, or a vast ocean, into small regions with the size of  $L$  even when the source region in total is very large. Also, surface waves usually dominate over body waves in real records, indicating the importance of the far field term. We here numerically investigate the assumption that the gradient of the bathymetry is small,  $|h_1 \nabla \xi| \ll 1$ . We consider that the bathymetry locally has the slope characterized by  $\partial h / \partial x = \tan \phi$ . In deriving eq. (8), we approximate  $[1 + (\partial h / \partial x)^2]^{-1/2} (\partial h / \partial x) \approx \partial h / \partial x$ . Fig. 5 compares  $[1 + (\partial h / \partial x)^2]^{-1/2} (\partial h / \partial x)$  and  $\partial h / \partial x$  as functions of the angle  $\phi$ , showing that the difference between the two functions is within 10 per cent when the angle is smaller than  $25^\circ$ . We may consider the gradient of the bathymetry is small in the formulation when the slope is smaller than  $25^\circ$ .

This study has considered two types of sea-bottom topography: a seamount and a randomly fluctuating sea bottom. When we suppose a seamount, an ocean wave with a specific wavelength characterized by  $\lambda \sim 2.2d$  can effectively interact with the topography. This simple model would be useful to understand the underlying process for the Love wave excitation mechanism. On the other hand, when we suppose a random sea-bottom fluctuation characterized by the von Karman-type PSDF, we can easily adjust the range of the wavenumber that can efficiently excite Love waves by changing the value of  $\kappa$  and  $a$ . This flexibility would be useful when we interpret the real records in the light of the model. The von Karman-type PSDF is an example in stochastic modelling of the bathymetry. We employed it because it shows a power law in the wavenumber domain as the real sea-bottom bathymetry (e.g. Fox & Hayes 1985; Goff & Jordan 1988; Turcotte 1989). Another reason is that it has the analytical representations both in the wavenumber and spatial domains (e.g. Sato & Fehler 1998), which sufficiently ensures the existence of the inverse Fourier transform of the PSDF and then the realization of  $\xi(x, y)$  in the spatial domain. The analytical representation of the von Karman type PSDF can provide the better perspectives for the Love-wave excitation mechanism. Our formulation,

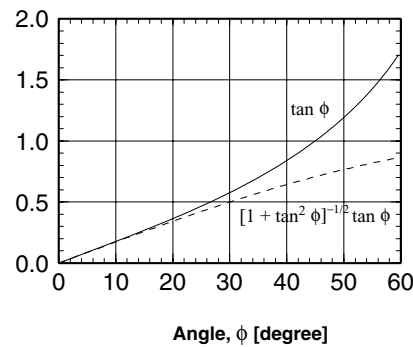


**Figure 5.** Functions  $\tan \phi$  (solid line) and  $[1 + \tan^2 \phi]^{-1/2} \tan \phi$  (dashed line).

on one hand, does not limit the type of PSDF until eq. (20). Eq. (20) holds for any function of the PSDF. For example, the PSDF characterized by two or three different powers can be another candidate for realistic modelling of the bathymetry (e.g. Fox & Hayes 1985; Goff & Tucholke 1997). Also, in some areas, sea-bottom topography clearly shows a preferred orientation (anisotropic PSDF), such as an ocean ridge or a trench (e.g. Goff & Jordan 1988). Eq. (20) also holds for an anisotropic PSDF in 2-D space (e.g. Saito 2006a, b).

## 5 CONCLUSIONS

This study has theoretically studied the Love wave excitation due to the interaction between propagating ocean wave and sea-bottom topography. By assuming a Fraunhofer diffraction range, or that the distance from the sea-bottom topography to an observation point is much greater than the spatial extent of the sea-bottom fluctuation, I derived an equivalent point force given by eq. (15) for the Love-wave excitation. The equivalent point force acts in the same direction as the propagation direction of the ocean wave. The excited Love wave has a radiation pattern characterized by  $\sin \theta$  where  $\theta$  is the angle between the propagation directions of the Love and ocean waves. The efficiency of the excitation is then investigated by employing both deterministic and stochastic models for sea-bottom topography. When a seamount given by a Gaussian function is used as a deterministic model, the equivalent point force has a narrow peak against the wavenumber of the ocean wave; a strong interaction occurs at  $\lambda = 2.2d$  where  $\lambda$  is the ocean-wave wavelength and  $d$  is the characteristic scale of the seamount. On the other hand, when randomly fluctuating sea-bottom topography characterized by a power-law spectrum is used, the interaction can occur over a wide range of the ocean wave wavelength.

## ACKNOWLEDGMENT

Careful reading of the manuscript and constructive comments by M. Korn and anonymous reviewers were very valuable for revision.

## REFERENCES

- Aki, K. & Richards, P., 2002. *Quantitative Seismology*, 2nd edn, University Science Books, California.
- Carrier, G.F., 1970. Stochastically driven dynamical systems, *J. Fluid Mech.*, **44**, 249–264.
- Chernov, L.A., 1960. *Wave Propagation in a Random Medium*, (English translation by R.A. Silverman), McGraw-Hill, New York.
- Friederich, A., Krüger, F. & Klinge, K., 1998. Ocean-generated microseismic noise located with the Gräfenberg array, *Journal of Seismology*, **2**, 47–64.
- Fox, C.G. & Hayes, D.E., 1985. Quantitative methods for analyzing the roughness of the seafloor, *Rev. Geophys.*, **23**, 1–48.
- Fukao, Y., Nishida, K., Suda, N., Nawa, K. & Kobayashi, N., 2002. A theory of the Earth's background free oscillations, *J. geophys. Res.*, **107**(B9), 2206, doi:10.1029/2001JB0001.
- Fukao, Y., Nishida, K. & Kobayashi, N., 2010. Seafloor topography, ocean infragravity waves and background Love and Rayleigh waves, *J. geophys. Res.*, doi:10.1029/2009JB006678.
- Gerstoft, P., Fehler, M.C. & Sabra, K.G., 2006. When Katrina hit California, *Geophys. Res. Lett.*, **33**, L17308, doi:10.1029/2006GL027270.
- Goff, J.A. & Jordan, T.H., 1988. Stochastic modeling of seafloor morphology: in version of sea beam data for second-order statistics, *J. geophys. Res.*, **93**, 13 589–13 608.
- Goff, J.A. & Tucholke, 1997. Multiscale spectral analysis of bathymetry on the flank of the mid-Atlantic ridge: modification of the seafloor by mass wasting and sedimentation, *J. geophys. Res.*, **102**, 15 447–15 462.
- Hasselmann, K.A., 1963. A statistical analysis of the generation of microseisms, *Rev. Geophys.*, **1**, 177–210.
- Harjes, H.P. & Seidl, D., 1978. Digital recording and analysis of broadband seismic data at the Gräfenberg (GRF) array, *J. geophys. Res.*, **44**, 511–523.
- Kobayashi, N. & Nishida, K., 1998. Continuous excitation of planetary free oscillations by atmospheric disturbances, *Nature*, **395**, 357–360.
- Kurrle, D. & Widmer-Schmid, R., 2008. The horizontal hum of the Earth: a global background of spheroidal and toroidal modes, *Geophys. Res. Lett.*, **35**, L06304, doi:10.1029/2007GL033125.
- Longuet-Higgins, M.S., 1950. A theory of the origin of microseisms, *Phil. Trans. R. Soc. Lond., A*, **243**, 1–35.
- Maeda, T., Sato, H. & Nishimura, T., 2008. Synthesis of coda wave envelopes in randomly inhomogeneous elastic media in a half-space: single scattering model including Rayleigh waves, *Geophys. J. Int.*, **172**, 130–154, doi:10.1111/j.1365-246X.2007.03603.x.
- Matsuzawa, T., Obara, K. & Maeda, T., 2008. Global propagation of cyclone-induced seismic wave from the Atlantic detected by the high-sensitivity accelerometers of Hi-net, Japan, *American Geophysical Union, Fall Meeting 2008*, abstract #S41C-1854.
- Mysak, L.A., 1978. Wave propagation in random media, with oceanic applications, *Rev. Geophys. Space Phys.*, **16**, 233–261.
- Nawa, K., Suda, N., Fukao, Y., Sato, T., Aoyama, Y. & Shibuya, K., 1998. Incessant excitation of the Earth's free oscillations, *Earth Planet. Space*, **50**, 3–8.

- Nishida, K. & Kobayashi, N., 1999. Statistical features of Earth's continuous free oscillations, *J. geophys. Res.*, **104**, 28 741–28 750.
- Nishida, K. & Fukao, Y., 2007. Source distribution of Earth's background free oscillations, *J. geophys. Res.*, **112**, B06306, doi:10.1029/2006JB004720.
- Nishida, K., Kawakatsu, H., Fukao, Y. & Obara, K., 2008. Background Love and Rayleigh waves simultaneously generated at the Pacific Ocean floors, *Geophys. Res. Lett.*, **35**, L16307, doi:10.1029/2008GL034753.
- Obara, K., 2002. Hi-net: high sensitivity seismograph network, Japan, *Lect. Notes Earth Sci.*, **98**, 79–87.
- Rhie, J. & Romanowicz, B., 2004. Excitation of Earth's continuous free oscillations by atmosphere-ocean-seafloor coupling, *Nature*, **431**, 552–556.
- Rhie, J. & Romanowicz, B., 2006. Study of the relation between ocean storms and the Earth's hum, *Geochem. Geophys. Geosys.*, **7**, Q10004, doi:10.1029/2006GC001274.
- Saito, T., 2006a. Synthesis of scalar-wave envelopes in two-dimensional weakly anisotropic random media by using the Markov approximation, *Geophys. J. Int.*, **165**, 501–515, doi:10.1111/j.1365-246X.2006.02896.x.
- Saito, T., 2006b. Velocity shift in two-dimensional anisotropic random media using the Rytov method, *Geophys. J. Int.*, **166**, 293–308, doi:10.1111/j.1365-246X.2006.02976.x.
- Saito, T. & Furumura, T., 2009a. Scattering of linear long-wave tsunamis due to randomly fluctuating sea-bottom topography: coda excitation and scattering attenuation, *Geophys. J. Int.*, **177**, 958–965, doi:10.1111/j.1365-246X.2009.03988.x.
- Saito, T. & Furumura, T., 2009b. Three-dimensional tsunami generation simulation due to sea-bottom deformation and its interpretation based on the linear theory, *Geophys. J. Int.*, **178**, 877–888, doi:10.1111/j.1365-246X.2009.04206.x.
- Sato, H. & Fehler, M., 1998. *Seismic Wave Propagation and Scattering in the Heterogeneous Earth*, AIP. Press/Springer Verlag, New York.
- Snieder, R., 1986. 3-D Linearized scattering of surface waves and a formalism for surface wave holography, *Geophys. J. R. astr. Soc.*, **84**, 581–605.
- Stoker, J.J., 1958. *Water Waves: The Mathematical Theory with Applications*, John Wiley and Sons, Inc., New York.
- Suda, N., Nawa, K. & Fukao, Y., 1998. Earth's background free oscillations, *Science*, **279**, 2089–2091.
- Tanimoto, T., 2005. The oceanic excitation hypothesis for the continuous oscillations of the Earth, *Geophys. J. Int.*, **160**, 276–288.
- Tanimoto, T., 2007. Excitation of normal modes by non-linear interaction of ocean waves, *Geophys. J. Int.*, **168**, 571–582.
- Tanimoto, T., Um, J., Nishida, K. & Kobayashi, N., 1998. Earth's continuous oscillations observed on seismically quiet days, *Geophys. Res. Lett.*, **25**, 1553–1556.
- Turcotte, D.L., 1989. Fractals in geology and geophysics, *Pure appl. Geophys.*, **131**, 171–196.
- Webb, S.C., 2008. The Earth's hum: the excitation of Earth normal modes by ocean waves, *Geophys. J. Int.*, **174**, 542–566.